Control Design of Modular Multilevel Converters in Normal and AC Fault Conditions for HVDC grids

Eduardo Prieto-Araujo[a], Adrià Junyent-Ferré[b], Carlos Collados-Rodríguez[a], Gerard Clariana-Colet[a], Oriol Gomis-Bellmunt[a]

[a] *Centre d'Innovació Tecnològica en Convertidors Estàtics i Accionaments (CITCEA-UPC), Departament d'Enginyeria Elèctrica, Universitat Politcnica de Catalunya. ETS d'Enginyeria Industrial de Barcelona Av. Diagonal, 647, Pl. 2. 08028 Barcelona, Spain*

[b] *Department of Electrical and Electronic Engineering, Imperial College London, South Kensington Campus, London SW7 2AZ, UK.*

Abstract

This paper describes a control design strategy of Modular Multilevel Converters (MMC) for High Voltage Direct Current (HVDC) applications to operate during normal and AC fault conditions. First, a steady state analysis of the converter is performed to identify the uses of the current components within the control strategy. Based on the initial stationary study, a complete converter control structure is proposed, which enables full control of the MMC internal energy during normal and AC fault conditions. A detailed design procedure is included for the current and energy regulators, in order to be able to ensure a dynamic response under any grid condition. Finally, theoretical developments are validated through simulation results by means of a detailed model in normal operation and during an AC voltage sag.

Keywords: HVDC transmission, Modular Multilevel Converters, Voltage-Source Converters, unbalanced operation.

1. Introduction

Classic Line Commutated Converter (LCC) High Voltage Direct Current (HVDC) transmission is a well established technology for long distance bulk power transmission [1]. However, the new Voltage Source Converter (VSC) HVDC technology is gaining market due to its black-start capability and independent control of active and reactive power, its suitability to operate in weak Alternating Current (AC) networks and the ability to design compact substations enabling offshore use [2].

VSCs are common in low and medium power motor drives and renewable generation systems. Typically, a VSC uses Insulated-Gate Bipolar Transistors (IGBT), enabling a controlled two or three-level voltage output driven by Pulse Width Modulation (PWM) [3]. This is not well suited for high voltage applications as the rated voltage of IGBTs is limited to a few kilovolts. Some

Email address: eduardo.prieto-araujo@citcea.upc.edu. Tel. +34 934016727 Fax. +34 934017433 (Eduardo Prieto-Araujo)

manufacturers chain multiple IGBTs to create high voltage switches; however, this requires a sophisticated drive circuit that is not easy to scale for very high voltages. To overcome this problem, Modular Multilevel Converters (MMC) were first proposed in [4] and different topologies have been adopted by different manufacturers since then [5–7]. MMC is foreseen as the technology of choice for VSC-HVDC. Besides enabling higher voltages, they have several additional benefits such as reduced harmonic content, reduced transformer dv/dt stress and great potential for standardization.

Unlike two-level VSCs, MMCs combine a large number of individually-controlled sub-modules (see Fig. 1) rather than chained IGBTs, requiring a sophisticated control structure. When compared to former well-known converter topologies, the MMC is more challenging to control due to its use of combined AC and DC current and voltage waveforms which have different roles in regulating the energy of the converter. These roles are not obvious but must be fully utilized in order to ensure that the converter can operate under all possible scenarios, including those with asymmetrical network voltages.

Two main types of control structures can be defined for MMCs [8], namely the direct and the indirect modulation [8]. The direct modulation strategy does not require energy balancing algorithms to operate, although it causes circulating currents flowing through the circuit [9]. Its performance can be improved by controlling the SM capacitor voltages [10–14] and/or suppressing the circulating currents [10, 15–19]. On the other hand, indirect modulation requires an energy balancing system to ensure a stable operation of the MMC [8]. Two different methods can be distinguished, the closed loop method [20–22] and the open loop method [23].

The aforementioned works mainly consider balanced AC grid operation. Other publications specifically deal with the operation under unbalanced AC grid voltage conditions. In [24], Guan et al. analyze the performance of the MMC during unbalanced AC faults, focusing on the control of the AC positive, negative and zero sequence and its impact on the converter variables. Regarding direct modulation strategies, in [25] a DC voltage ripple suppression method is proposed to eliminate second-order harmonics in the DC bus voltage. Also, [26] describes an advanced regulator for the different circulating current components that appear during an unbalanced voltage sag. In [27] the authors analyze the impact of an unbalanced voltage sag over the converter energies. Shaohua et. al. [28] describe analytically the components of the circulating current during AC faults, besides proposing a Proportional Resonant (PR) controller to eliminate them. In [29] a DC voltage ripple suppression control is proposed, which is combined with the circulating current control to enhance the fault-tolerant capability of the converter. In [30] a negative sequence current controller, able to operate the system in open loop, is explained. Then, in [31] a control strategy to balance the arm currents using common zero-sequence voltage is proposed for converters supplying passive networks.

Moving to MMC closed loop control strategies, [32] describes an enhanced energy control methodology which is able to improve the system dynamics when the MMC is operating under non-stiff DC link voltage conditions. Also, [33] details an energy based controller able to operate an MMC-based HVDC link under a Single Line to Ground (SLG) fault in one of the terminals, ensuring its stability and fast dynamics. Focused also in SLG faults, [34] proposes a control method combining both a normal and a fault operation modes, with a seamless transition between them. Furthermore, other articles are focused on specific AC voltage conditions that could impose restrictions on the energy balancing control on the converters. In [35] and [36], the operation of

the converter under these conditions is analyzed, detailing different solutions to be able to stabilize the converter.

As detailed above, a number of prior publications have proposed different ad-hoc modifications to the closed loop energy-based control strategies for MMCs. However, to the best of the authors knowledge, these control proposals do not include a complete control dynamic design procedure able to ensure the behavior of the MMC in case of a power transient or an unbalanced voltage sag. This article details a step-by-step design of the MMC control, starting from the basic equations and ending with a complete energy regulation scheme, able to operate in any grid condition.

First, an in-depth steady-state analysis of the system is conducted, which enables an intuitive understanding of the role of the different degrees of freedom of current and voltage components in the converter. Based on this steady-state analysis, specific current components are selected to regulate specific degrees of freedom of the converter. Then, a current controller design is performed to ensure an adequate dynamic response for both AC and DC current components within the same circuit, which is required for the arms current regulation. Then, a simple reference calculation technique is detailed for both grid and circulating currents considering an unbalanced AC grid voltage operation. Besides, the dynamic design of the six energy controllers (one per converter arm) is addressed in order to be able to maintain the energy stored in the converter arms within the operational limits during both steady-state and transient conditions.

The article is organized as follows: Section 2 describes the converter and its characteristic equations. Then, in Section 3 a steady state analysis of the converter is developed, further identifying the uses of the current components within the converter control in Section 4. In Section 5 the different parts of the converter control are described and the current and energy regulators are designed. Finally, in Section 6 simulation results to validate the proposed control design in normal operation and during a voltage sag are presented.

2. System description

The MMC has N_{arm} sub-modules (SM) in each arm[1]. These can be controlled individually to either insert their capacitor in series with the arm or to bypass it, which allows the arm to behave as a controllable voltage source fed from an aggregated capacitor-based energy storage device [15]. The voltage of the arms can be used to control the current flowing through the converter. The target current is chosen to achieve the desired exchange of power between the AC grid and the DC grid as well as maintaining the internal energy balance of the converter. To represent the converter [37], the circuit equations can be obtained per each phase j ($j = a, b, c$)

$$V_u^{DC} - v_u^j - v_g^j - v_n = R_a i_u^j + L_a \frac{di_u^j}{dt} + R_s i_s^j + L_s \frac{di_s^j}{dt} \tag{1}$$

$$-V_l^{DC} + v_l^j - v_g^j - v_n = -R_a i_l^j - L_a \frac{di_l^j}{dt} + R_s i_s^j + L_s \frac{di_s^j}{dt} \tag{2}$$

where R_a and L_a are the resistance and inductance of the arm inductor respectively, R_s and L_s correspond to the phase inductor, V_u^{DC} and V_l^{DC} are the voltages of the upper and the lower halves

[1]Each phase of the converter is commonly called a *leg*; whereas the upper and the lower halves of a leg are commonly called *arms* (see Fig. 1).

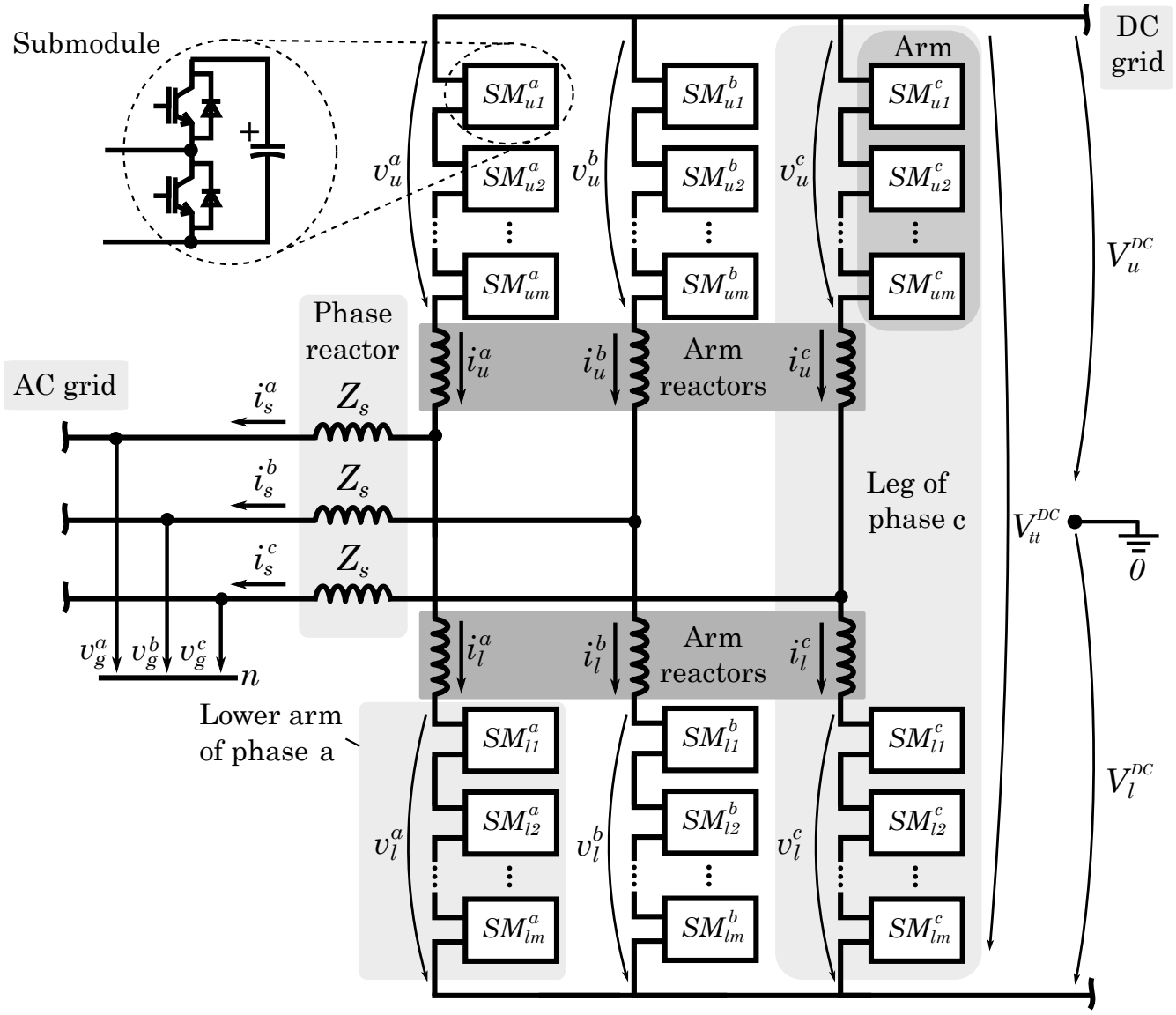

Figure 1: Complete scheme of an MMC converter

of the HVDC link, v_g^j is the AC grid voltage, v_u^j and v_l^j are the voltages applied by the upper and the lower arms respectively, i_u^j and i_l^j are the currents flowing through the upper and lower arms respectively and i_s^j is the AC grid current. Further, the following variables and parameters are defined

$$\begin{cases} v_{diff}^j \triangleq \frac{1}{2}(-v_u^j + v_l^j) \\ v_{sum}^j \triangleq v_u^j + v_l^j \\ i_{sum}^j \triangleq \frac{1}{2}(i_u^j + i_l^j) \\ R \triangleq R_s + \frac{R_a}{2} \\ L \triangleq L_s + \frac{L_a}{2} \end{cases} \quad \text{and} \quad \begin{cases} v_u^j = -v_{diff}^j + \frac{1}{2}v_{sum}^j \\ v_l^j = v_{diff}^j + \frac{1}{2}v_{sum}^j \\ i_u^j = \frac{1}{2}i_s^j + i_{sum}^j \\ i_l^j = -\frac{1}{2}i_s^j + i_{sum}^j \end{cases} \tag{3}$$

where v_{diff}^j and v_{sum}^j are the differential and the additive voltages applied by the converter respectively and i_{sum}^j is the additive (inner) current, which is common to the upper and lower arms. Adding and subtracting equations (1) and (2), while applying the aforementioned variable change, leads to

$$\underbrace{\frac{1}{2}(V_u^{DC} - V_l^{DC})}_{\triangleq V_{off}^{DC}} + v_{diff}^j - v_g^j - v_n = R\, i_s^j + L\, \frac{di_s^j}{dt} \tag{4}$$

$$v_{sum}^j - \underbrace{(V_u^{DC} + V_l^{DC})}_{\triangleq V_t^{DC}} = -2R_a i_{sum}^j - 2L_a \frac{di_{sum}^j}{dt} \tag{5}$$

where V_{off}^{DC} is half the imbalance between the voltage of positive and the negative HVDC poles. This will normally be close to zero but can be large under pole-to-ground faults in the HVDC grid. Also, note that (4) is related to AC side current i_s^j, whereas (5) is related to additive currents i_{sum}^j.

Then, assuming that no neutral connection is available

$$i_s^a + i_s^b + i_s^c = 0 \tag{6}$$

This can be combined with the summation of (4) over $j = a, b, c$ to obtain the voltage of the neutral point v_n

$$v_n = \underbrace{\frac{1}{3}(v_{diff}^a + v_{diff}^b + v_{diff}^c)}_{\triangleq v_{diff}^0} - \underbrace{\frac{1}{3}(v_g^a + v_g^b + v_g^c)}_{\triangleq v_g^0} + V_{off}^{DC} \tag{7}$$

Note that v_{diff}^0 is controlled by the converter but does not produce any current. This is normally exploited by VSCs to extend the AC output voltage range using third harmonic voltage injection [38]. Due to symmetry, (4) and (5) can be written in vector form by combining a, b and c as

$$v_{diff}^{abc} - v_g^{abc} + (V_{off}^{DC} - v_n)\begin{bmatrix}1 & 1 & 1\end{bmatrix}^T = \mathbf{R}\, i_s^{abc} + \mathbf{L}\, \frac{di_s^{abc}}{dt} \tag{8}$$

$$v_{sum}^{abc} - V_t^{DC}\begin{bmatrix}1 & 1 & 1\end{bmatrix}^T = -2\mathbf{R_a} i_{sum}^{abc} - 2\mathbf{L_a} \frac{di_{sum}^{abc}}{dt} \tag{9}$$

where $\mathbf{R}$, $\mathbf{R_a}$, $\mathbf{L}$ and $\mathbf{L_a}$ are 3x3 diagonal matrices with R, R_a, L and L_a terms at the diagonal, respectively.

3. Steady state analysis

The voltage applied by the converter arms and the current flowing through them contain both AC and DC components. These play different roles in the power exchange between the AC and DC networks and the energy stored in the converter itself. In order to better understand these roles, it is useful to perform a decoupled AC and DC steady state analysis of the circuit. Next, this analysis is detailed distinguishing between AC and DC components for both the grid and inner currents.

3.1. AC analysis

For the AC analysis, assuming V_{off}^{DC} is purely DC, equation (8) can be expressed in the phasor domain as:

$$\underline{V}_{diff}^{abc} - \underline{V}_{g}^{abc} - \underline{V}_{n}\begin{bmatrix}1 & 1 & 1\end{bmatrix}^{T} = \underline{\mathbf{Z}}\,\underline{I}_{s}^{abc} \tag{10}$$

where $\underline{\mathbf{Z}}$ is 3x3 diagonal matrix with the term $R + j\omega L$ at the diagonal[2]. It is convenient to apply the Fortescue transformation to the former equation [39]. The Fortescue transformation $\underline{\Theta}^{+-0}$ of a phasor vector $\underline{\Theta}^{abc}$ is defined as

$$\underline{\Theta}^{+-0} \triangleq \mathbf{F}\underline{\Theta}^{abc} = \frac{1}{3}\begin{bmatrix}1 & \underline{p}^2 & \underline{p} \\ 1 & \underline{p} & \underline{p}^2 \\ 1 & 1 & 1\end{bmatrix}\underline{\Theta}^{abc}$$

with $\underline{p} = e^{j\frac{-2\pi}{3}}$. Multiplying equation (10) by $\mathbf{F}$ leads to

$$\underline{I}_{s}^{+-} = \underline{Z}^{-1}\left[\underline{V}_{diff}^{+-} - \underline{V}_{g}^{+-}\right] \tag{11}$$

As noted earlier, the zero sequence component of the current flowing towards the AC grid is zero and therefore can be removed from the result. The current flowing towards the AC network, $\underline{I}_{s}^{+-}$, is used to exchange power with the AC network and can be controlled using the differential voltage, $\underline{V}_{diff}^{+-}$. In addition, multiplying the phasor domain expression of (9) by $\mathbf{F}$ yields

$$\underline{I}_{sum}^{+-0} = -\frac{1}{2\underline{Z}_{a}}\underline{V}_{sum}^{+-0} \tag{12}$$

where $\underline{Z}_a$ is the arm impedance $R_a + j\omega L_a$. The positive and negative sequence components of the additive current $\underline{I}_{sum}^{+-}$ can be used to exchange energy between the upper and the lower halves of the converter to achieve internal balance while the zero component $\underline{I}_{sum}^{0}$ should be kept close to zero to avoid AC voltage distortion in the DC network.

3.2. DC analysis

The DC analysis is performed equating the derivatives of current in (8) and (9) to zero. As with the AC analysis, it is convenient to distinguish between the zero sequence component and

[2] ω is the grid frequency

the rest of the current. In the DC case, this can be done by using the Clarke transformation [40], which is defined as

$$\Theta^{\alpha\beta 0} \triangleq \mathbf{C}\Theta^{abc} = \frac{1}{3}\begin{bmatrix} 2 & -1 & -1 \\ 0 & -\sqrt{3} & \sqrt{3} \\ 1 & 1 & 1 \end{bmatrix} \Theta^{abc} \tag{13}$$

Transforming the steady state DC form of (8), assuming that the DC grid voltage $V_g^{\alpha\beta DC}$ is zero, leads to

$$V_{diff}^{\alpha\beta DC} = R\, I_s^{\alpha\beta DC} \tag{14}$$

As in the AC case, the zero sequence component of I_s is strictly zero; however, the remaining DC current $I_s^{\alpha\beta DC}$ can flow through the transformer windings and must be kept equal to zero in order to avoid undesired core saturation. This can be controlled using $v_{diff}^{\alpha\beta DC}$. In addition, applying (13) to the steady state DC form of (9) leads to

$$I_{sum}^{\alpha\beta DC} = -\frac{1}{2R_a} V_{sum}^{\alpha\beta DC} \tag{15}$$

and

$$I_{sum}^{0DC} = \frac{1}{2R_a}(V_t^{DC} - V_{sum}^{0DC}) \tag{16}$$

The zero sequence component of the additive DC current is used to exchange power between the converter and the DC network and can be controlled using V_{sum}^{0DC}. On the other hand, $I_{sum}^{\alpha\beta DC}$ is controlled through $V_{sum}^{\alpha\beta DC}$ and can be used to exchange energy between different legs of the converter to achieve internal energy balance. This will be important under severe voltage unbalances in the AC network, where the power exchanged by different legs will be significantly different.

4. Converter current components uses

In this section, a summary description of the MMC current components and their corresponding uses within the converter is included, distinguishing between grid I_s^{abc} and inner currents I_{sum}^{abc}.

- Grid AC current components I_s. These currents can be expressed in *abc* magnitudes or in the Fortescue domain $+-0$, in order to decouple the positive and negative sequence components from the zero sequence component.
  - Grid AC positive and negative sequence currents I_s^{+-}. These currents must be regulated continuously in order to establish an active/reactive power transfer between the converter and the AC grid.
  - Grid AC zero sequence current I_s^0. This component is zero due to the three-wire connection of the converter.
- Grid current DC components $I_s^{\alpha\beta 0DC}$. These currents can be expressed in *abc* magnitudes or in the Clarke domain $\alpha\beta 0$ in order to decouple the converter $\alpha\beta$ current components from the zero sequence component.

  - Grid DC $\alpha\beta$ currents $I_s^{\alpha\beta DC}$. These currents should be regulated to zero to avoid DC currents flowing through the AC grid, which could cause saturation of magnetic components.
  - Grid DC zero sequence current I_s^{0DC}. This component is zero due to the three-wire connection of the converter.

- Inner AC current components I_{sum}^{+-0}. These currents can be expressed in *abc* magnitudes or in the Fortescue domain $+-0$ in order to decouple the positive and negative circulating sequence components from the zero sequence component.
  - Inner AC positive and negative sequence currents I_{sum}^{+-}. These components are used to compensate energy deviations between the upper and lower arms. An energy unbalance may appear transiently during a power flow change or an AC voltage variation, and steadily during an eventual DC pole voltage imbalance.
  - Inner AC zero sequence current I_{sum}^{0}. This component must be controlled to zero in order to avoid an AC current component flowing through the DC link. Note that, the AC zero sequence component is different from the DC zero sequence component, which is related with the DC link power transmission.

- Inner current DC components $I_{sum}^{\alpha\beta 0DC}$. These currents can be expressed in *abc* magnitudes or in the Clarke domain $\alpha\beta 0$ in order to decouple the converter $\alpha\beta$ circulating currents from the zero sequence component.
  - Inner DC $\alpha\beta$ currents $I_{sum}^{\alpha\beta DC}$. During an unbalanced voltage sag, each phase unit exchanges a different amount of power with the AC grid, which is causing a sustained unbalance in the energy stored within the converter legs. These DC current $\alpha\beta$ components are used to balance the energy stored in the converter legs during these type of faults.
  - Inner DC zero sequence current I_{sum}^{0DC}. This component is directly related with the current flowing through the DC link. It is different from zero, if the converter injects or absorbs power from the DC grid.

The nature and uses of each of the grid and current components are summarized in Table 1.

5. Converter control

In this section, a design methodology for the converter controllers is proposed based on the parameters shown in Table 2. An overview of the control structure proposed for the converter is shown in Fig. 2, detailing the different stages and possible operational modes.

The control strategy must be designed to meet several objectives:

- Control the different degrees of freedom of the MMC by means of specific current components.
- Control the AC and DC components of the grid and additive currents flowing through the converter.

Table 1: Converter current components and their uses

Comp.	**Freq.**	**Comp.**	**Use**
I_s	AC	+,-	Active and reactive current to the AC grid (continuous).
		0	Equal to 0 due to three-wire connection.
	DC	α,β	Controlled to zero to prevent DC current flowing through the AC grid.
		0	Equal to 0 due to three-wire connection.
I_{sum}	AC	+,-	Internal power exchange between upper and lower arms (transient).
		0	Controlled to zero to avoid AC distortion in the DC grid.
	DC	α,β	Internal power exchange between the legs of the converter (continuous/transient).
		0	Power flowing to the DC grid (continuous).

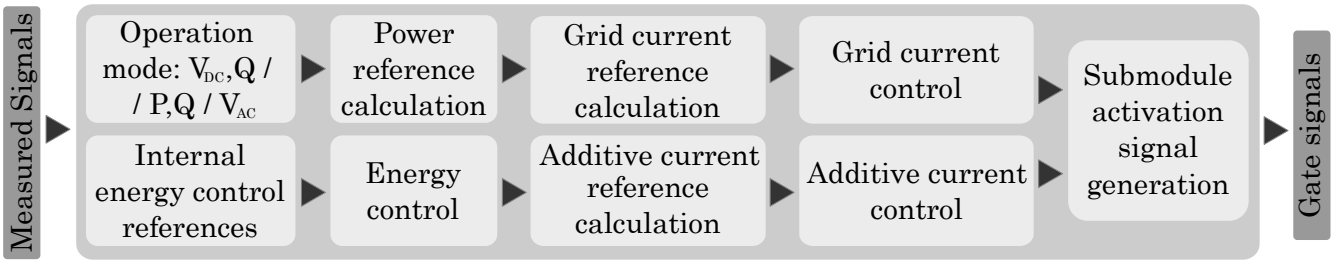

Figure 2: Overall MMC control structure

Table 2: System parameters for an example MMC

Parameter	**Symbol**	**Value**	**Units**
Rated power	S	526	MVA
Rated power factor	$\cos\varphi$	0.95 (c)	-
AC-side voltage	U	320	kV rms ph-ph
HVDC link voltage	V_{DC}	$\pm$320	kV
Phase reactor impedance	Z_s	j 0.05	pu
Arm reactor impedance	Z_a	0.01+j 0.2	pu
Converter sub-modules per arm	N_{arm}	400	sub-modules
Average sub-module voltage	V_{module}	1.6	kV
Sub-module capacitance	C_{module}	8	mF

- Establish a power exchange between the AC and the DC grid.
- Continuous balancing of the energy stored in the converter arms, avoiding large deviations.
- Enable the converter operation under any grid condition.

To meet these objectives, the following parts of the control structure are addressed:

- Grid and additive current reference calculation considering unbalanced AC grid voltage conditions.
- Design of the grid and additive current regulators to track AC and DC current references.
- Design of the energy regulators to balance the energy stored in the converter arms.

Based on this structure a complete control scheme can be implemented as shown in Fig. 3. Next, the design of each part of the structure is addressed in detail. The current reference calculation strategy (Fig. 3 green sector) is explained for both grid and inner currents in Section 5.1. The grid (Fig. 3 orange sector) and inner (Fig. 3 yellow sector) current control dynamic design is described in Section 5.2. Finally, the converter arm energy control (Fig. 3 blue sector) dynamic design is addressed in Section 5.3.

5.1. Current reference calculation

As in most VSC topologies, the control structure for an MMC consists of a high-level power and energy controller which produces current reference values for a nested current controller, which in turn gives output voltage commands to a switching signal generator (see Fig. 2). Although the calculation of current reference values has elements in common with that of a two-level converter, the greater number of degrees of freedom of the MMC makes it of greater complexity.

5.1.1. AC network current reference calculation

DC component of the AC network current. As discussed earlier, the zero sequence component of the AC network current is strictly zero due to the three-wire connection, and the reference of $I_s^{\alpha\beta DC}$ is set to zero and must be controlled to avoid transformer saturation.

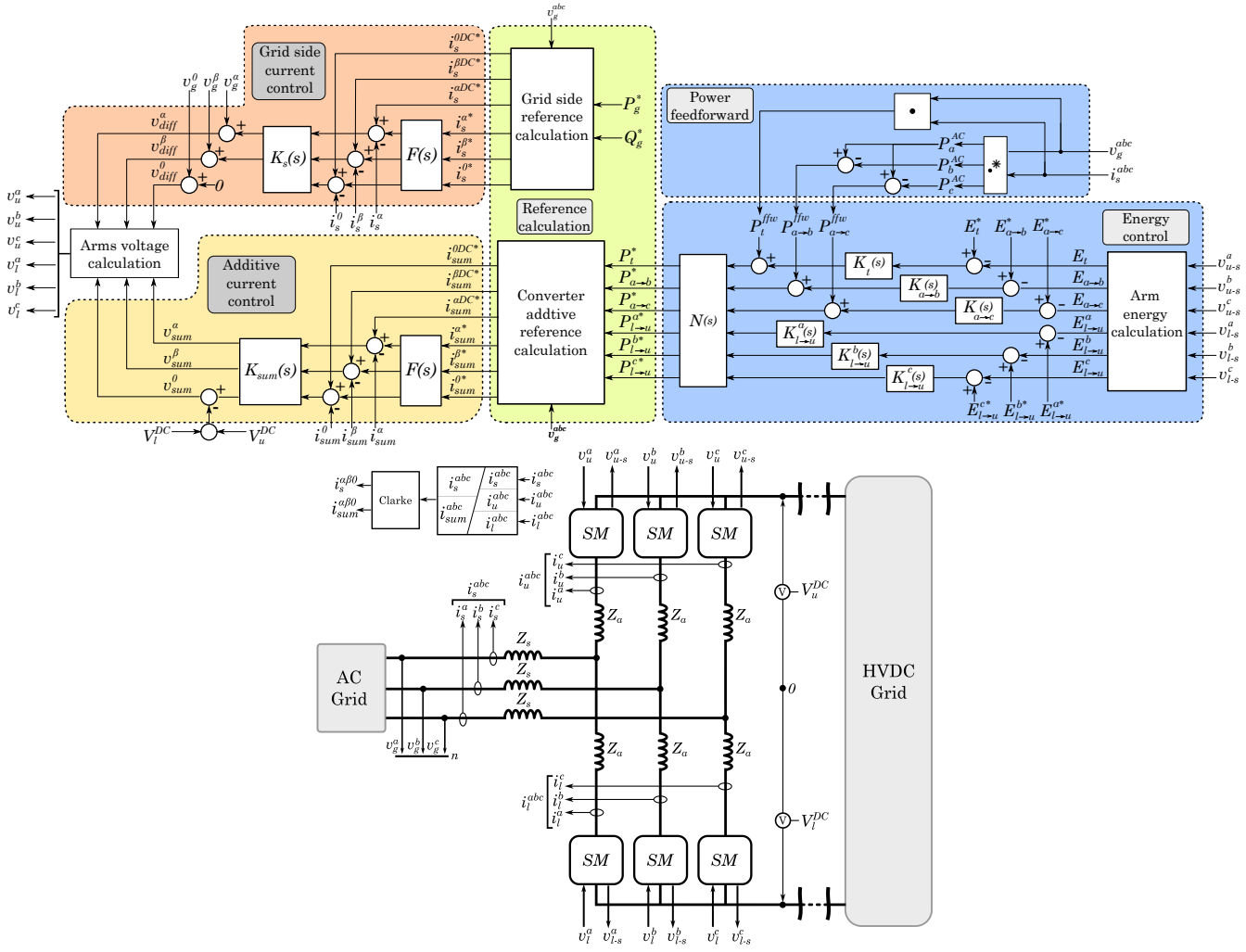

Figure 3: MMC control structure

AC component of the AC network current. The AC network current references can be calculated using the same methods as in classical two-level converters. Under balanced conditions, the two degrees of freedom of the current can be adjusted to obtain the desired active and reactive power exchange with the AC network [40]. However, when considering unbalanced AC network voltages several options exist [41], and the preferred solution has not been selected yet. The most common choice is to set the negative sequence current to zero and export only positive sequence current chosen to obtain the desired active and reactive power exchange. This causes an asymmetrical exchange of power between the AC network and the different legs of the converter even in steady state, which needs to be compensated by the converter to ensure internal energy balance. The calculation of the current reference is simplified by applying the so-called Park transformation matrix $\mathbf{T}(\theta)$ to voltage and current variables. The Park transformation is equivalent to the Clarke transformation combined with a rotation of angle θ and can be obtained as

$$\Theta^{qd0} = \underbrace{\mathbf{R}(\theta)\,\mathbf{C}}_{\mathbf{T}(\theta)}\,\Theta^{abc}; \quad \mathbf{R}(\theta) = \begin{bmatrix} \cos\theta & -\sin\theta & 0 \\ \sin\theta & \cos\theta & 0 \\ 0 & 0 & 1 \end{bmatrix} \tag{17}$$

Following the nomenclature introduced by Akagi [40, 42], the non-oscillatory terms of the instantaneous active and reactive power of the power exported to the AC grid, P_g and Q_g respectively, can be calculated from the positive voltage and current qd components as:

$$P_g = \frac{3}{2}\left(v_g^{q+} i_s^{q+} + v_g^{d+} i_s^{d+}\right); \quad Q_g = \frac{3}{2}\left(v_g^{q+} i_s^{d+} - v_g^{d+} i_s^{q+}\right) \tag{18}$$

Assuming v_g^{d+} to be zero, which can be granted if the angle of the Park transformation is chosen to match the angle of the positive sequence, the current references can be calculated as

$$i_s^{q^*} = \frac{2}{3}\frac{P_g^*}{v_g^{q+}}; \quad i_s^{d^*} = \frac{2}{3}\frac{Q_g^*}{v_g^{q+}} \tag{19}$$

This approach is sometimes known as the feed-forward method, as opposed to an alternative approach where the current reference is obtained from the output of a PI controller fed with the error between measured power and reference power. A discussion about their advantages and drawbacks can be found in [43]. If the converter is connected to a weak grid, the coupling between output current and grid voltage seen by the converter may require further consideration as shown in [44]. Finally, if the losses of the converter filter are not negligible, these can be included in the calculation of (19) for better accuracy [41].

5.1.2. Additive current reference calculation

DC component of the additive current. The zero sequence component of the DC additive current I_{sum}^{0DC} is used to export power from the converter to the DC grid P_t, whereas the rest of the DC additive current is used to exchange power between converter legs $P_{a\to b}$ and $P_{a\to c}$. It is convenient to define the following new power variables

$$P_{a\to b} \triangleq P_a - P_b, \quad P_{a\to c} \triangleq P_a - P_c, \quad P_t \triangleq \sum_{j=a,b,c} P_j \tag{20}$$

where $P_j \approx V_t^{DC} i_{sum}^{jDC}$.

Similarly to the case of the AC network current, the approximation above assumes the losses of the arm inductors to be negligible. This enables calculating the current references in the Clarke reference frame as

$$\begin{bmatrix} i_{sum}^{\alpha DC^*} \\ i_{sum}^{\beta DC^*} \\ i_{sum}^{0DC^*} \end{bmatrix} = \frac{1}{3\ V_t^{DC}} \begin{bmatrix} 0 & 1 & 1 \\ 0 & \sqrt{3} & -\sqrt{3} \\ 1 & 0 & 0 \end{bmatrix} \begin{bmatrix} P_t^* \\ P_{a\to b}^* \\ P_{a\to c}^* \end{bmatrix} \tag{21}$$

Under normal operation, most of the DC additive current will be zero sequence and it will be in charge of ensuring that the power exchanged between the converter and the AC network is equal to the power exchanged with the HVDC link. However, under severe voltage imbalances in the AC network, the DC additive current of phases a, b and c can be significantly different in order to compensate the power imbalance between phases.

AC component of the additive current. The AC voltage applied by the converter arms will be close to the AC network voltage. This can be seen from (11) given that $\underline{Z}$ is small. When comparing the AC voltage of the upper and the lower arms, they will have opposite signs. Therefore, the additive AC current $\underline{I}_{sum}^{+-}$ can be used to exchange power between the upper and lower arms of the converter. On the other hand, the zero sequence component $\underline{I}_{sum}^{0}$ must be set to zero to prevent AC current flowing to the HVDC link. Unlike the AC network current, the additive current can contain positive and negative sequence components with no impact on the AC grid. The power exchanged between upper and lower arms can be obtained by multiplying the AC arm voltage by the AC additive current. The AC arm voltage can be approximated as

$$v_l^{abc} \approx -v_u^{abc} \approx \sqrt{2} \begin{bmatrix} V_g^+ \cos(\omega t) + V_g^- \cos(\omega t + \psi) \\ V_g^+ \cos(\omega t - \frac{2\pi}{3}) + V_g^- \cos(\omega t + \psi + \frac{2\pi}{3}) \\ V_g^+ \cos(\omega t + \frac{2\pi}{3}) + V_g^- \cos(\omega t + \psi - \frac{2\pi}{3}) \end{bmatrix} \tag{22}$$

where ψ is the angle between the positive and the negative grid voltages. The AC additive current can be expressed as

$$i_{sum}^{abc} = \sqrt{2} \begin{bmatrix} I_{sum}^+ \cos(\omega t + \gamma) + I_{sum}^- \cos(\omega t + \alpha) \\ I_{sum}^+ \cos(\omega t + \gamma - \frac{2\pi}{3}) + I_{sum}^- \cos(\omega t + \alpha + \frac{2\pi}{3}) \\ I_{sum}^+ \cos(\omega t + \gamma + \frac{2\pi}{3}) + I_{sum}^- \cos(\omega t + \alpha - \frac{2\pi}{3}) \end{bmatrix} \tag{23}$$

where γ and α are the angles of the positive and negative sequence additive current respectively, taking the positive sequence grid voltage as the reference of angles. Multiplying arm voltages by the additive currents for phases a, b and c while eliminating the oscillatory terms at the double line frequency yields

$$P_{l\to u}^a(t) \;=\; V_g^- I_{sum}^+ \cos(\gamma - \psi) \;+\; V_g^+ I_{sum}^+ \cos\gamma \;+\; V_g^- I_{sum}^- \cos(\psi \;-\; \alpha) \;+\; V_g^+ I_{sum}^- \cos\alpha \tag{24}$$

$$P^b_{l\to u}(t) = V_g^- I^+_{sum}\cos\left(\gamma-\psi-\frac{4\pi}{3}\right) + V_g^+ I^+_{sum}\cos(\gamma)+ \\ + V_g^- I^-_{sum}\cos(\psi-\alpha) + V_g^+ I^-_{sum}\cos\left(\alpha+\frac{4\pi}{3}\right) \quad (25)$$

$$P^c_{l\to u}(t) = V_g^- I^+_{sum}\cos\left(\gamma-\psi+\frac{4\pi}{3}\right) + V_g^+ I^+_{sum}\cos(\gamma)+ \\ + V_g^- I^-_{sum}\cos(\psi-\alpha) + V_g^+ I^-_{sum}\cos\left(\alpha-\frac{4\pi}{3}\right) \quad (26)$$

Note that there are four parameters that need to be chosen (I^+_{sum}, I^-_{sum}, α and γ) in order to adjust three power variables ($P^a_{l\to u}$, $P^b_{l\to u}$ and $P^c_{l\to u}$). The redundant degree of freedom can be used for secondary purposes such as minimizing losses. Here, γ is chosen to be zero, thus the positive sequence current is chosen to be aligned with the positive sequence voltage. By introducing this condition, the former equations can be rewritten in a more compact form

$$\underbrace{\begin{bmatrix}P_1\\P_2\\P_3\end{bmatrix}}_{P} = \underbrace{\begin{bmatrix}V_g^+ & 0 & V_g^-\cos\psi\\ 0 & V_g^+ & -V_g^-\sin\psi\\ V_g^-\cos\psi & -V_g^-\sin\psi & V_g^+\end{bmatrix}}_{X}\underbrace{\begin{bmatrix}I^-_{sum}\cos\alpha\\ -I^-_{sum}\sin\alpha\\ I^+_{sum}\end{bmatrix}}_{I} \quad (27)$$

where the new power variables are defined as

$$\begin{aligned} P_1 &\triangleq \frac{1}{3}(-P^c_{l\to u} - P^b_{l\to u} + 2P^a_{l\to u}) \\ P_2 &\triangleq \frac{1}{3}(\sqrt{3}P^c_{l\to u} - \sqrt{3}P^b_{l\to u}) \\ P_3 &\triangleq \frac{1}{3}(P^a_{l\to u} + P^b_{l\to u} + P^c_{l\to u}) \end{aligned} \quad (28)$$

Based on the power references given by the energy controllers to maintain the energy balance between upper and lower arms, the current references can be obtained from (27) as

$$\underbrace{\begin{bmatrix}I^-_{sum}\cos\alpha\\ -I^-_{sum}\sin\alpha\\ I^+_{sum}\end{bmatrix}}_{I} = \underbrace{\frac{1}{(V_g^+)^2-(V_g^-)^2}\cdot\begin{bmatrix}M_{11} & M_{12} & M_{13}\\ M_{21} & M_{22} & M_{23}\\ M_{31} & M_{32} & M_{33}\end{bmatrix}}_{M}\underbrace{\begin{bmatrix}P_1\\P_2\\P_3\end{bmatrix}}_{P} \quad (29)$$

$$M_{11} = \frac{2(V_g^+)^2 + (\cos(2\psi)-1)(V_g^-)^2}{2V_g^+}$$

$$M_{22} = \frac{2(V_g^+)^2 + (-\cos(2\psi)-1)(V_g^-)^2}{2V_g^+}$$

$$M_{12} = M_{21} = -\frac{\sin(2\psi)(V_g^-)^2}{2V_g^+}; \quad M_{33} = V_g^+$$

$$M_{13} = M_{31} = -\cos(\psi)V_g^-; \quad M_{23} = M_{32} = \sin(\psi)V_g^-$$

This equation has a discontinuity when $V_g^+ = V_g^-$, resulting in very high current reference values when voltage sags with high imbalance occur. One way to overcome this problem is to disable the AC component of the additive current upon detecting such disturbance and enabling it once the fault is cleared [35]. Even though this makes the converter unable to control the balance between upper and lower arms during the sag, it is worth noting that there are no sources of sustained drift between upper and lower arms unless faults occur within the converter itself.

5.2. Current control

Although the equivalent circuit of the MMC is more complex than that of a two-level converter, by using the transformations introduced earlier it is possible to transform it into two separate circuits that can be controlled independently using well-known inverter control techniques. However, in the MMC, additive currents contain DC plus AC components and modulation techniques are prone to introduce disturbances in both domains. Therefore, the current controllers must be designed to track references and to reject AC and DC disturbances. Under such requirements, there is no advantage in transforming voltages and currents using the rotating Park matrix (17). Therefore, the Clarke transformation matrix (13) is applied in order to separate the zero sequence component from the rest. Applying (13) to (8) and (9) yields

$$v_{diff}^{\alpha\beta} - v_g^{\alpha\beta} = \mathbf{R}\, i_s^{\alpha\beta} + \mathbf{L}\, \frac{di_s^{\alpha\beta}}{dt} \tag{30}$$

$$v_{sum}^{\alpha\beta 0} - V_t^{DC} \begin{bmatrix} 0 & 0 & 1 \end{bmatrix}^T = -2\mathbf{R_a} i_{sum}^{\alpha\beta 0} - 2\mathbf{L_a} \frac{di_{sum}^{\alpha\beta 0}}{dt} \tag{31}$$

Note that all these equations are decoupled, therefore individual single-input single-output (SISO) controllers can be used for each of them. Here, the current controller of choice is a two-degree of freedom structure with a conventional PI controller and an AC reference pre-filter $F(s)$ [45]. The control structure is shown in Fig. 3, in the grid and additive current control part. This strategy enables the controller to track both AC and DC references with the desired tracking error. The parameters of the PI controllers are chosen using an inverse-based design [46] where the PI is set to cancel out the current dynamics and to introduce an integrator that enables achieving the desired performance. In the case of the AC network current, the transfer function of the controller $K_s(s)$ is defined as

$$K_s(s) = \frac{k_{p-s}s + k_{i-s}}{s}, \quad k_{p-s} = \frac{L}{\tau_s}, \quad k_{i-s} = \frac{R}{\tau_s} \tag{32}$$

where τ_s is the resulting closed-loop time constant which is normally chosen in the range of few milliseconds [47]. The same controller structure $K_{sum}(s)$ can be used for the additive currents, by choosing

$$K_{sum}(s) = \frac{k_{p-sum}s + k_{i-sum}}{s},\ k_{p-sum} = \frac{2\,L_a}{\tau_{sum}},\ k_{i-sum} = \frac{2\,R_a}{\tau_{sum}} \tag{33}$$

Once the current controller has been defined, the AC reference pre-filter is calculated to compensate the deviation applied by the closed loop controller. The pre-filter $F(s)$ is a lead compensator that

corrects the gain M_t and phase M_p deviation at the grid frequency ω, as

$$F(s) = \alpha K_f \frac{s+\omega_1}{s+\omega_2}; \quad \alpha = \frac{1+M_p}{1-M_p}; \quad \begin{cases} \omega_1 = \omega/\sqrt{\alpha} \\ \omega_2 = \omega\sqrt{\alpha} \end{cases} \tag{34}$$

$$K_f = \frac{1}{M_t\, M_f}; \quad M_f = \sqrt{\frac{1+M_p}{1-M_p}} \tag{35}$$

As an example, the grid current controller is designed according to the parameters in Table 2 to track references in 10 ms (settling time). Fig. 4 presents the bode diagram relating the DC (Fig. 4a) and AC (Fig. 4b) component reference with the respective current components, showing that the controller is able to track AC and DC current references with 0 dB and 0 phase delay.

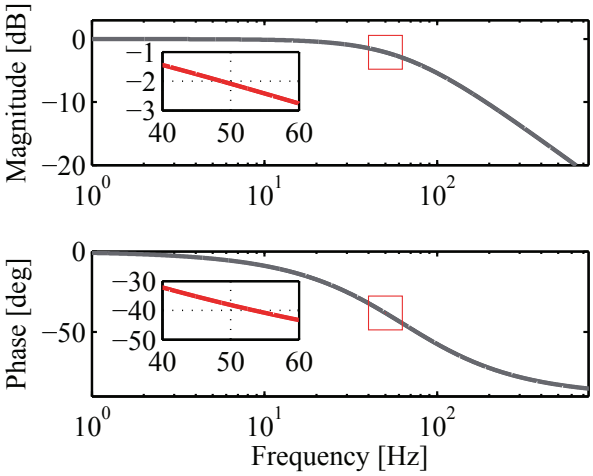

(a)

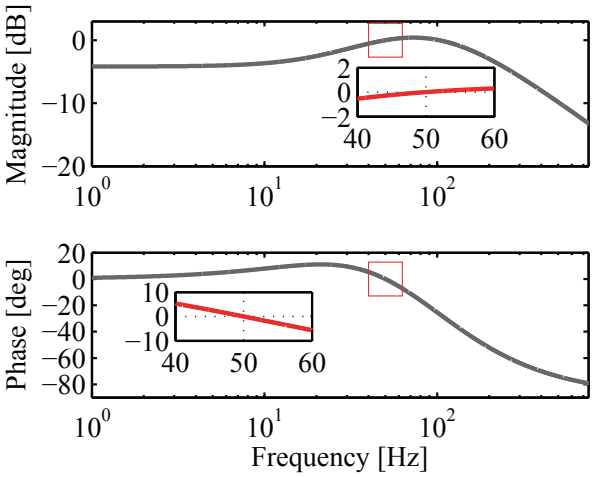

(b)

Figure 4: Closed loop transfer function for the grid current controller. a) DC current regulation: without an AC reference pre-filter. b) AC current regulation: with an AC reference pre-filter.

5.3. Energy Control

The energy regulators of the MMC sit on top of the additive current controllers. There are six energy variables (as many as arms in the MMC) controlled by six different regulators. It is useful to define a new set of energy variables, which will be controlled using the converter additive currents

$$E_t = \sum_{j=a,b,c} E_u^j + \sum_{j=a,b,c} E_l^j \tag{36}$$

$$E_{a\to b} = (E_u^a + E_l^a) - (E_u^b + E_l^b) \tag{37}$$

$$E_{a\to c} = (E_u^a + E_l^a) - (E_u^c + E_l^c) \tag{38}$$

$$E_{l\to u}^j = E_l^j - E_u^j \tag{39}$$

where E_t is the total energy stored in the converter, $E_{a\to b}$ and $E_{a\to c}$ are the differences of energy between legs a and b and a and c respectively, and $E_{l\to u}^j$ is the difference of energy between the upper and lower arms of leg j with $j = a, b, c$. These are linear combinations of the total energy stored in the arms, which can be approximated as [17]

$$E_u^j \approx \frac{1}{2}\frac{C_{module}}{N_{arm}}\left(v_{u-s}^j\right)^2; \quad E_l^j \approx \frac{1}{2}\frac{C_{module}}{N_{arm}}\left(v_{l-s}^j\right)^2 \tag{40}$$

where v_{u-s}^j and v_{l-s}^j are the sums of the capacitor voltages of all sub-modules of the upper and lower converter arms, respectively.

In order to achieve sustained operation, energy differences between legs and between upper and lower arms must be regulated to zero while the total energy of the converter must be regulated to its rated value, given by

$$E_t^* = 6 \cdot \frac{1}{2}\frac{C_{module}}{N_{arm}}\left(N_{arm} \cdot V_{module}\right)^2 \tag{41}$$

where V_{module} is the nominal voltage of each sub-module.

5.3.1. Total energy and energy differences between legs

The total energy of the arms E_t is affected by the mismatch between the power exchanged with the AC network and the DC network. Then, although the total energy could be regulated using the AC or the DC power references, it is normally controlled using the DC power reference P_t^*. In addition, the energy differences between legs $E_{a\to b}$ and $E_{a\to c}$ are caused by the differences between the active power exchanged by each converter leg under AC network voltage imbalances. These differences can be controlled using the DC power exchanged between legs $P_{a\to b}^*$ and $P_{a\to c}^*$.

The energy controller structure can be seen in Fig. 3 within the energy control part. These controllers are composed of a feedback term, plus a feed-forward term corresponding to the power exchanged by each converter leg with the AC grid P_j^{AC}, expressed in terms of the total power exchanged P_t^{ffw} and the differences between legs $P_{a\to b}^{ffw}$ and $P_{a\to c}^{ffw}$, as

$$P_j^{AC} \approx v_g^j\, i_s^j \tag{42}$$

$$P_{a\to b}^{ffw} \triangleq P_a^{AC} - P_b^{AC}, \quad P_{a\to c}^{ffw} \triangleq P_a^{AC} - P_c^{AC} \tag{43}$$

$$P_t^{ffw} \triangleq \sum_{j=a,b,c} P_j^{AC} \tag{44}$$

To design the controllers, a simplified scheme of the system is depicted in Fig. 5. The transfer function between power and energy is an integrator, while the transfer function between power references and actual power $G_{i_{sum}}(s)$ can be modeled as a first-order system with unit gain and a time constant set according to the design specifications of the additive current controllers. The feed-forward loop includes a first-order low-pass filter $F_{fw}(s)$ to avoid exceeding the bandwidth of the additive current controller. Moreover, a notch filter $N(s)$ is also included to avoid that the controller attempts to compensate the energy oscillations due to the natural AC ripple.

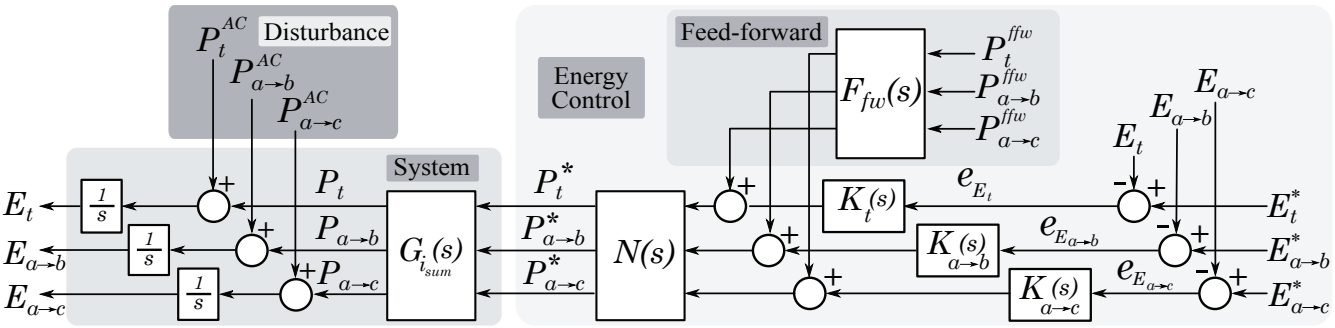

Figure 5: Simplified scheme to design the energy regulators to balance the total energy of the converter and the energy differences between the converter legs

The following 2^{nd} order notch filter structure can be used to cancel a specific frequency

$$N_{\omega_n}(s) \triangleq \frac{s^2 + \omega_n^2}{1 + 2\omega_n/Q + \omega_n^2} \tag{45}$$

where ω_n is the AC frequency to be avoided and Q is the quality factor of the filter. In this case, $N(s)$ is chosen as a series combination of $N_{\omega}(s)$ and $N_{2\omega}(s)$ in order to cancel line and double-line frequencies. The effect of choosing different values of Q is shown in Fig. 6. Here, a quality factor of 3 is chosen, which shows good performance filtering the AC components without a significant degradation of the time response.

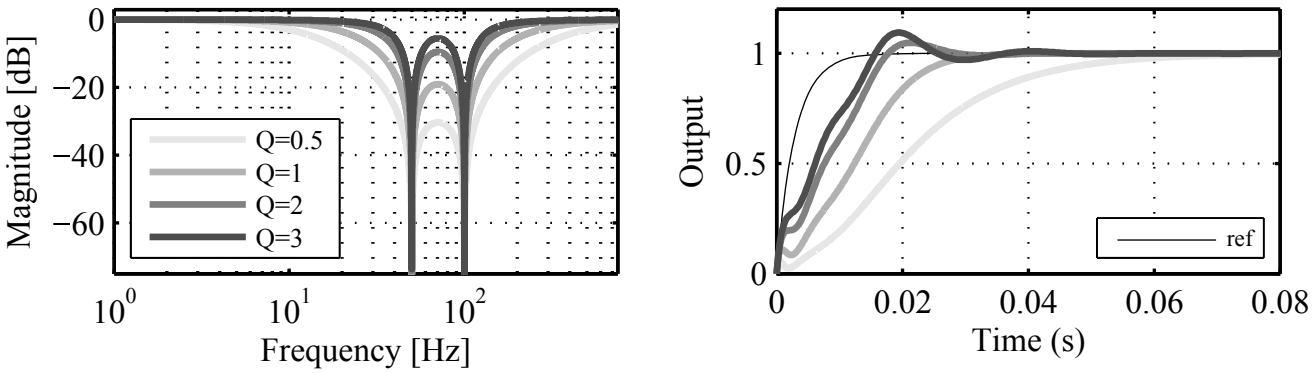

Figure 6: Bode plot (left) and step response (right) of the notch filter used for canceling line and double-line frequencies

The energy controllers are designed considering a disturbance rejection problem through a loop shaping strategy. The control specifications are:

- Maximum energy allowed error: 10% of the rated total energy.
- Settling time of 1 s to achieve a ±2% deviation from the set-point value, after a power disturbance.

Based on these requirements, a tentative frequency response of the system can be defined. For the three controllers, the worst-case scenario disturbance assumed is a step change of the nominal power. Hence, as the system plant to be controlled (Fig. 5) and the worst disturbance input are equivalent, the regulators employed to control E_t, $E_{a\to b}$ and $E_{a\to c}$ are also equivalent. To design them, the relevant transfer function to be analyzed is the one that relates the power disturbances (P_t^{AC}, $P_{a\to b}^{AC}$ and $P_{a\to c}^{AC}$) with its corresponding energy error (e_{E_t}, $e_{E_{a\to b}}$ and $e_{E_{a\to c}}$), typically named SG_d [45]. Then, a maximum gain imposed to this transfer function can be defined based on the maximum disturbance input (500 MW) and the maximum energy error (10% deviation)

$$|SG_{d_{max}}| = 20\log_{10}\frac{e_{max}}{d_{max}} = 20\log_{10}\frac{0.1\cdot E_t^*}{500\cdot 10^6} \approx -46 \text{ dB} \tag{46}$$

In addition, the low corner frequency of SG_d is chosen to be 1 rad/s, in order to achieve the desired settling time. Based on these boundaries, the shadowed area in Fig. 7a is defined. Then, the parameters of the controller can be selected to fit within the defined area. To verify the design methodology, in Fig. 7b the response of the designed controller for a nominal power step response is included, showing that the disturbance is rejected in 1 second without exceeding the maximum defined error.

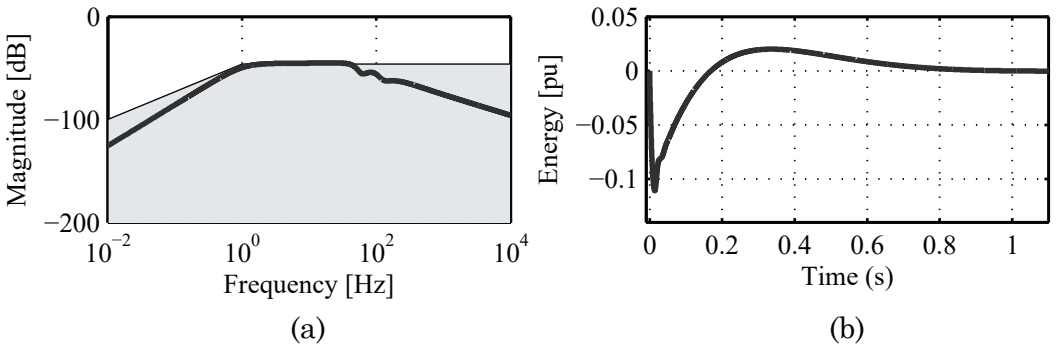

Figure 7: Bode diagram and step response of SG_d transfer function

5.3.2. Energy differences between upper and lower arms

Imbalanced AC grid voltages are not a source of sustained drift of the differences between the energy stored in the upper and lower arms. However, small amount of error may still appear during transients, which favors the inclusion of a feedback controller. The plant to be controlled (shown in Fig. 8) has a similar structure to that of the total energy (see Fig. 5); therefore, the regulator design methodology employed is equivalent.

6. Case study

In this section, different simulations are carried out in Matlab Simulink® to validate the dynamic design of the proposed controller. The system parameters used for this study are shown in Table 2. Next, the different conducted simulation studies are detailed:

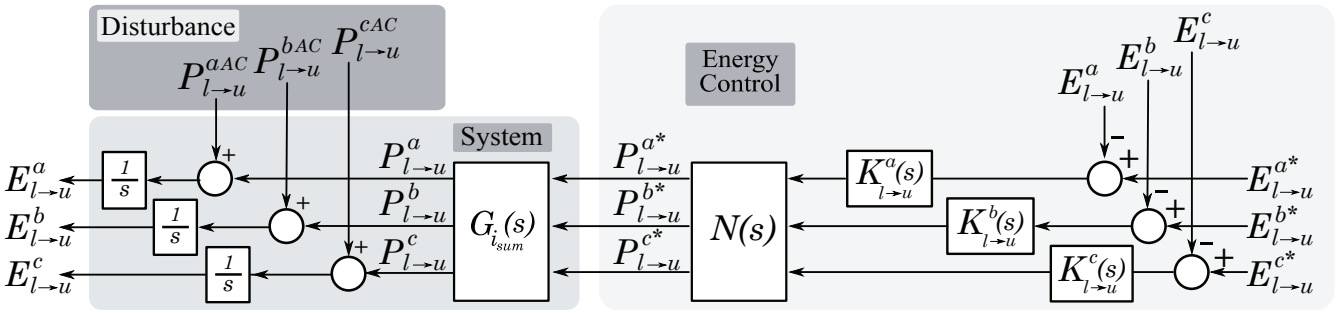

Figure 8: Simplified scheme to design the energy regulators to balance the upper and lower arms of the converter

- Power step change response of the converter under normal conditions.
- Unbalanced voltage sag operation while injecting nominal power.
- Comparison of the proposed controller with other control methods.

All results are shown in per unit values according to Table 3 base values.

Table 3: System base values

Magnitudes	**Symbol**	**Value**	**Units**
Base power	S_b	526	MVA
Base DC voltage	V_b^{DC}	640	kV
Base AC voltage	V_b^{AC}	320	kV rms ph-ph
Base DC current	I_b^{DC}	821	A
Base AC current	I_b^{AC}	949	A

6.1. Simulation model description

The MMC model used for the simulations is built based on the accelerated model proposed in [48]. This model allows to access to each individual sub-module voltage and provides enough accuracy compared to a complete model [49]. Each sub-module is represented by a capacitor that is charged or discharged depending on its switching state and the current that is flowing through its arm. The modulation technique implemented is the Nearest Level Control (NLC) technique [50], which calculates the number of active sub-modules in each arm and uses a reduced switching frequency strategy to increase the efficiency of the converter.

6.2. Normal operation mode

Fig. 10 shows the converter response to a power reference set-point change from 0 to nominal power (injecting to the AC grid) at time 1 s. The power reference is changed following a first order system evolution with a settling time constant of 100 ms [47]. A detailed legend for the color codes in Figs. 10, 11, 12, 13 and 14 is shown in Fig. 9. It can be observed that the converter AC and DC power reach the steady state in the defined time. Fig. 10 confirms that the total sum of the energy of the arms is affected. However, the energy controller is able to compensate the effect without important deviations.

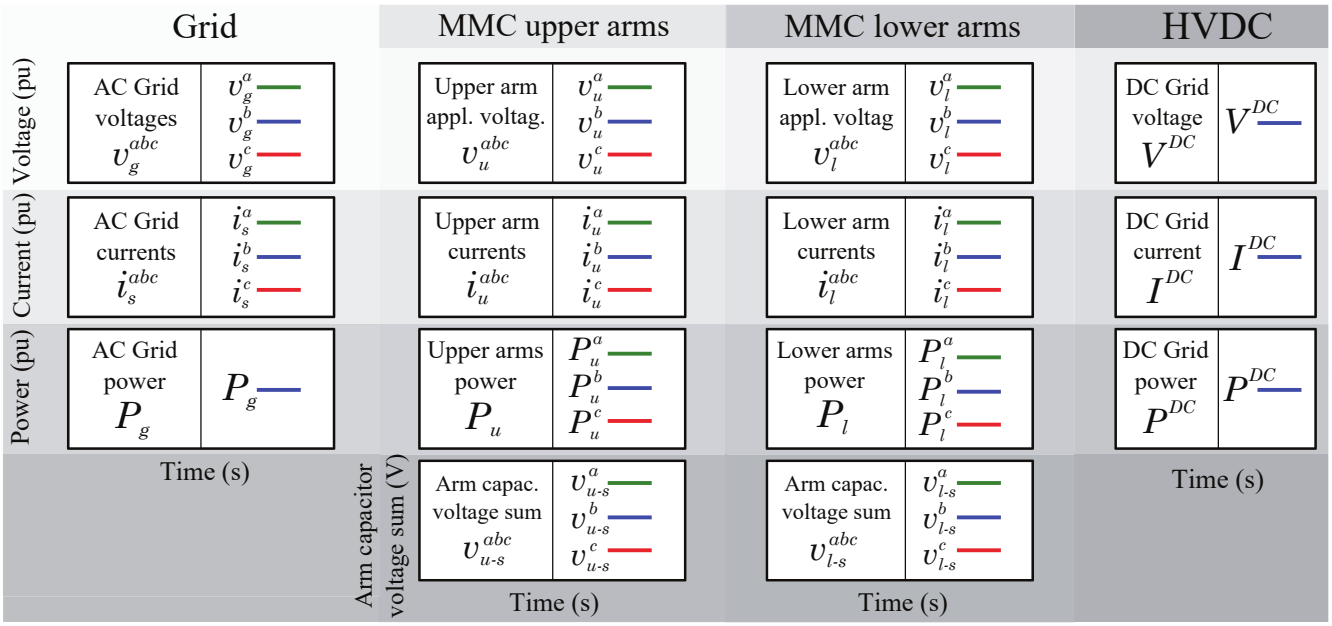

Figure 9: Graphs detailed legend for the simulation results

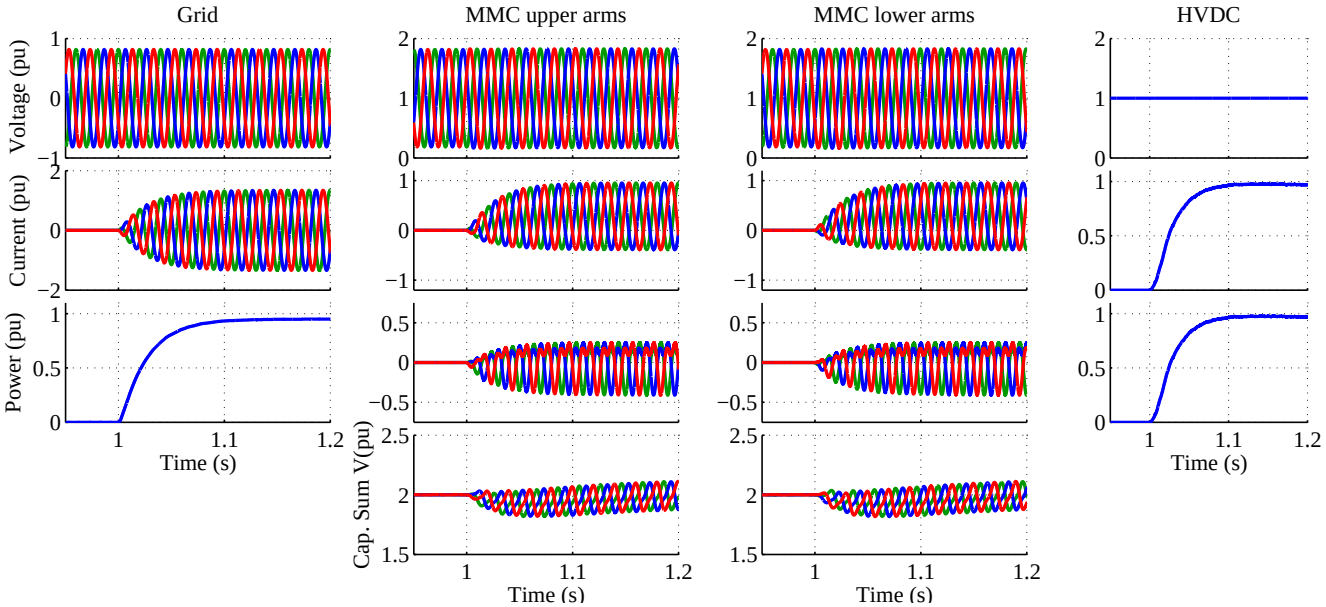

Figure 10: Simulation results of a nominal power step change

6.3. Unbalanced voltage sag

Fig. 11 and Fig. 12 show the converter response to an asymmetrical type G voltage sag [51], considering a remaining positive sequence voltage of 0.5 pu and a negative sequence voltage of 0.25 pu. The simulated voltage sag starts at time 3 s and the voltage is fully restored at time 5 s. Although in a real network, a deep and highly unbalanced voltage sag condition would be sustained for less than 250 ms [52], in this case, the sag has been extended for 2 s to validate the controller stability.

Note that the converter only injects positive sequence current. Due to the voltage imbalance, the power injected to the grid presents an oscillatory component at double line frequency. The power injection is reduced by the same ratio as the positive sequence voltage of the grid. Besides, the remaining converter current capacity is employed to inject reactive current to the grid, as required by grid codes [53]. It can be observed that the total sum of the capacitor voltages (converter energy) is affected by the voltage sag (see Fig. 11). However, the proposed controllers are able to regulate the converter energy back to their normal state. Finally, Fig. 12 shows how the converter goes back to its initial state upon clearing the fault without a significant deviation.

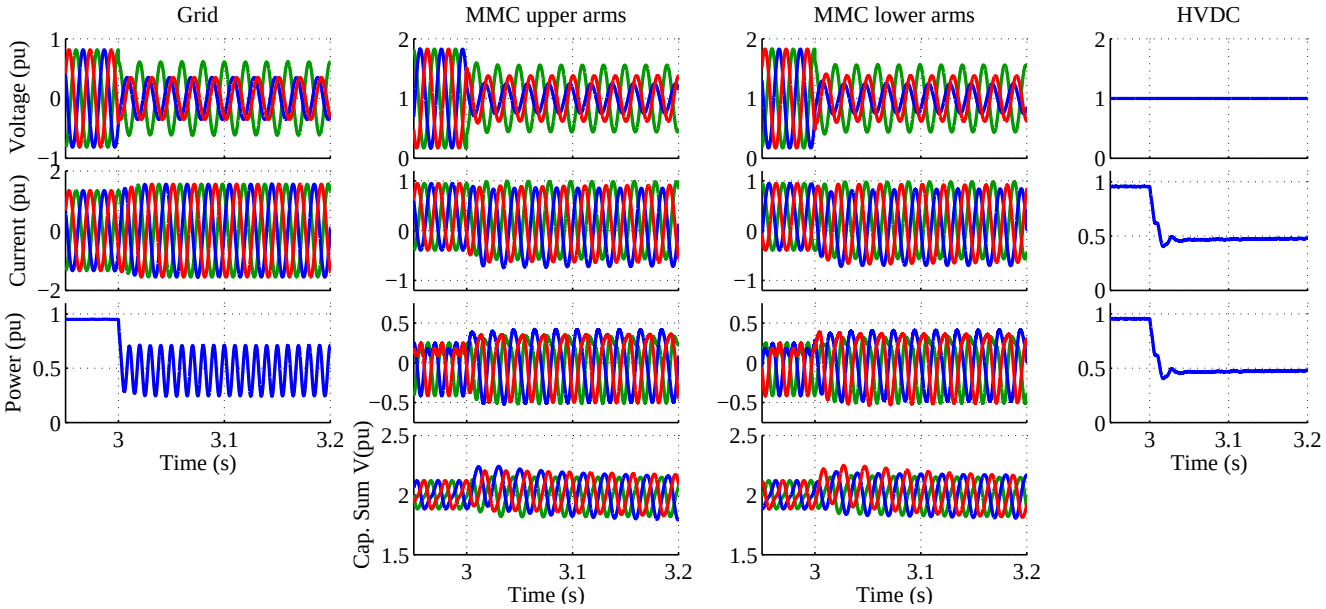

Figure 11: Simulation results of an asymmetrical voltage sag

6.4. Comparison with other control methods

In this section, a comparison between the proposed control strategy and two other well-known controllers is carried out. The first controller (C1) [15] consists of a direct modulation strategy including a circulating current control suppression. The second strategy (C2) [20] is based on a closed loop energy control strategy (equivalent to the proposed one). Both strategies include a decoupled positive and negative grid current controller [54], which is able to maintain the negative sequence at zero, while supporting the grid using only positive sequence current. Next, both MMC control strategies are simulated under the previous defined voltage sag conditions. Note that, the

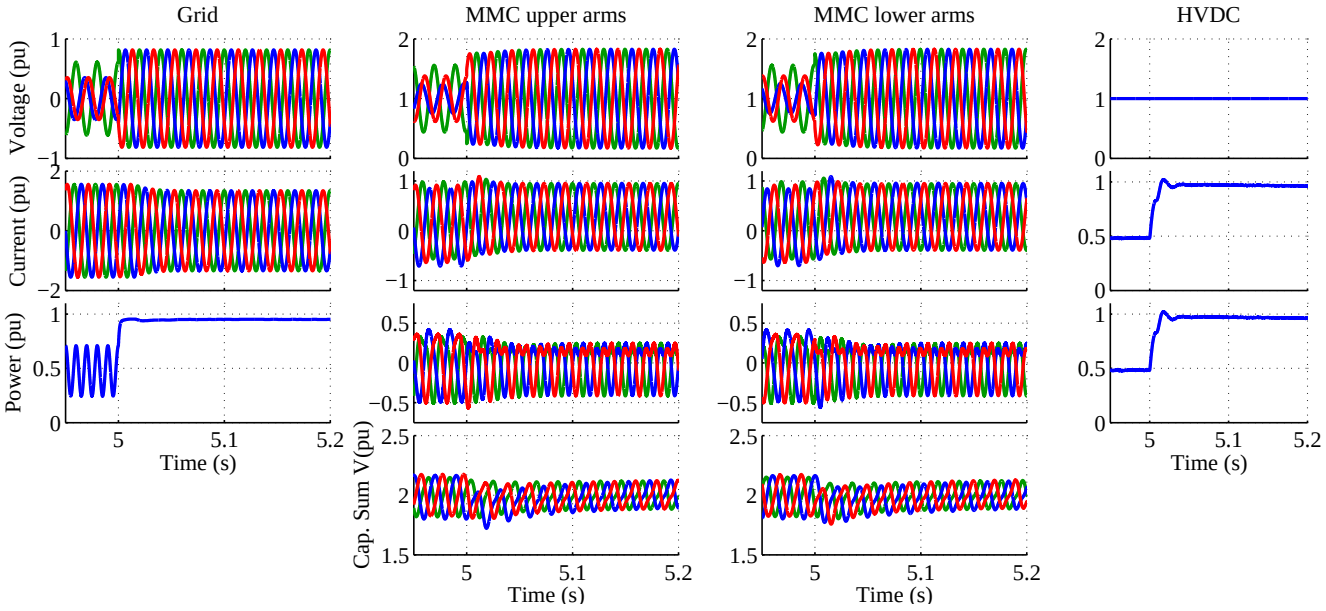

Figure 12: Simulation results of an asymmetrical voltage sag

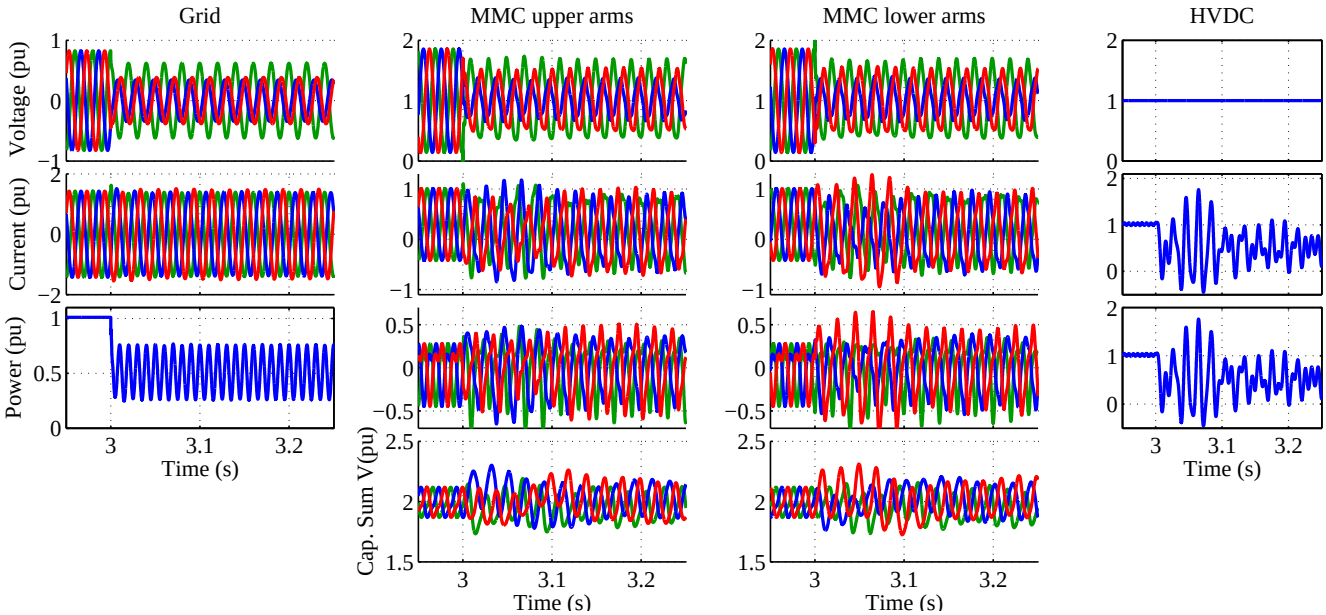

Figure 13: Simulation results of an asymmetrical voltage sag for control strategy C1 [15]

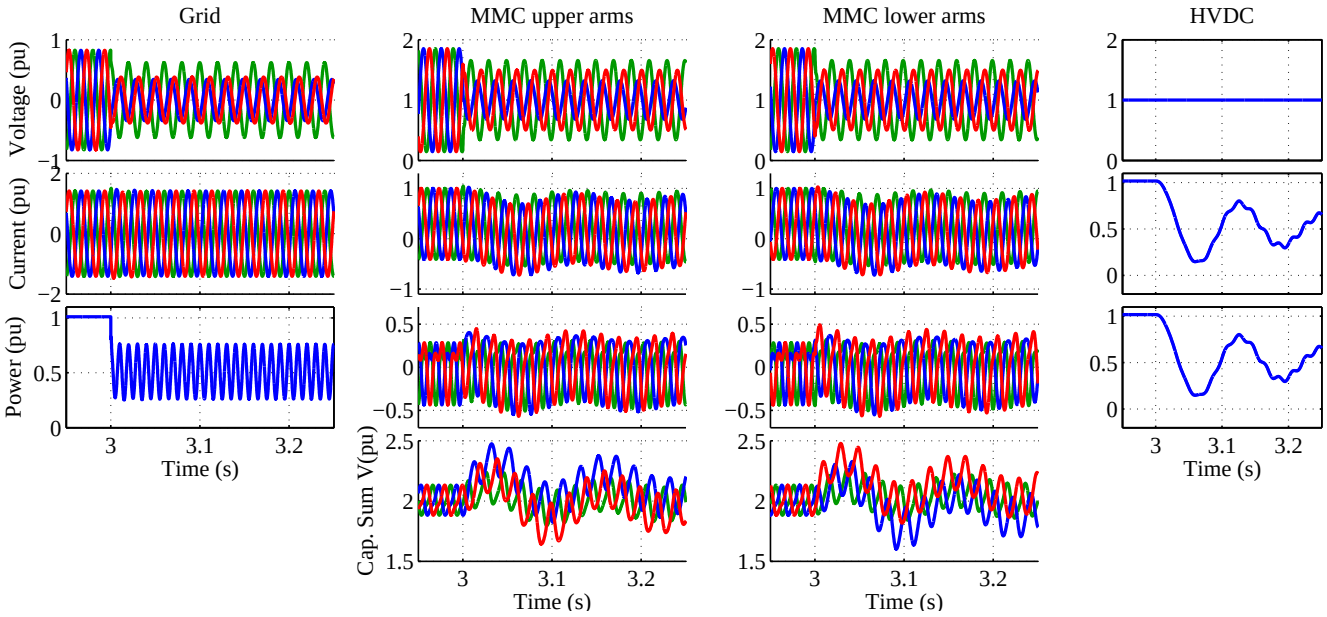

Figure 14: Simulation results of an asymmetrical voltage sag for control strategy C2 [20]

design of the controllers has been optimized in order to obtain the best possible response of the system.

Fig. 13 shows the behavior of the direct modulation strategy presented in [15]. It can be seen that the AC grid currents are balanced due to the action of the decoupled positive and negative sequence current regulator (1st column - 2nd row of Fig. 13), obtaining similar results to the control proposed in this paper (see Fig. 11). However, focusing on the converter inner and DC side magnitudes, it is observed that the DC current and power appear completely distorted (last column of Fig. 13). This transient is reflected in the converter upper and lower arm currents and in the total sum of the arm capacitor voltages (last row of Fig. 13), showing a larger ripple compared to the simulation results shown in Fig. 11. According to these results, the converter would be eventually disconnected due to the large current and power transients.

Fig. 14 shows the response of the closed loop control structure described in [20], which is conceptually closer to the strategy proposed in this article. As in the previous case, the AC side results are equivalent (1st column - 2nd row of Fig. 14), due to the decoupled positive and negative sequence controller. Focusing on the DC side, the transient observed in the DC current and power (last column of Fig. 14) is much slower than the one shown by the proposed concept (see Fig. 11), as the current is not controlled ensuring a dynamic response. This power difference between the AC and DC exchanged power causes an important oscillation of the total capacitor arm voltage (last row of Fig. 14), which may lead to the disconnection of the converter, if the sub-modules voltage limitations are exceeded.

Essentially, the main difference between C1 and C2 and the methodology presented in this paper is the inner control of the converter. The response of the converter towards the AC grid is equivalent in the three cases. However, the proposed controller achieves much better regulation of the inner dynamics of the converter by means of a current controller in combination with an adequate reference calculation strategy and an energy controller that is able to minimize the energy

deviations.

7. Conclusion

A control structure for the half-bridge-cell based MMC to operate in any grid condition has been presented. First, a steady state analysis of the converter is carried out to identify the current components to be used to regulate the converter degrees of freedom. Based on this analysis, a complete reference calculation strategy to obtain the grid and additive current references from the corresponding power references is described, also considering unbalanced grid conditions. To apply these current references, current regulators are designed to be able to track both AC and DC current components. Finally, regulators to balance the converter arms stored energy are designed using simplified models of the converter. With the proposed control structure, the converter is able to operate despite the grid conditions, maintaining the converter balanced. The control strategy proposed is validated through simulations under both normal and unbalanced grid conditions.

Acknowledgements

This work was supported by the *Ministerio de Economía y Competitividad* under the projects ENE2013-47296 and ENE2015-67048-C4-1-R.

References

[1] M. Bahrman, B. Johnson, The abcs of hvdc transmission technologies, IEEE Power and Energy Magazine 5 (2) (2007) 32–44.

[2] O. Gomis-Bellmunt, J. Liang, J. Ekanayake, R. King, N. Jenkins, Topologies of multiterminal HVDC-VSC transmission for large offshore wind farms, Electric Power Syst. Res. 81 (2) (2011) 271–281.

[3] B. Bose, Power Electronics And Motor Drives: Advances and Trends, Elsevier Science, 2010.

[4] A. Lesnicar, R. Marquardt, An innovative modular multilevel converter topology suitable for a wide power range, in: IEEE Power Tech Conf. Proc, 2003, Bologna, Vol. 3, 2003, pp. 6 pp. Vol.3–. doi:10.1109/PTC.2003.1304403.

[5] J. Dorn, H. Huang, D. Retzmann, A new multilevel voltage-sourced converter topology for hvdc applications, CIGRE Session. Paris, France: Int. Council on Large Electric Syst. (2008) 1–8.

[6] B. Jacobson, P. Karlsson, G. Asplund, L. Harnefors, T. Jonsson, Vsc-hvdc transmission with cascaded two-level converters, in: Cigré session, 2010, pp. B4–B110.

[7] M. Merlin, T. Green, P. Mitcheson, D. Trainer, D. Critchley, R. Crookes, A new hybrid multi-level voltage-source converter with dc fault blocking capability, in: 9th IET Int. Conf. on AC and DC Power Transmission, 2010. ACDC., 2010, pp. 1–5. doi:10.1049/cp.2010.0987.

[8] S. Debnath, J. Qin, B. Bahrani, M. Saeedifard, P. Barbosa, Operation, control, and applications of the modular multilevel converter: A review, IEEE Transactions on Power Electronics 30 (1) (2015) 37–53. doi:10.1109/TPEL.2014.2309937.

[9] D. Siemaszko, A. Antonopoulos, K. Ilves, M. Vasiladiotis, L. ngquist, H. P. Nee, Evaluation of control and modulation methods for modular multilevel converters, in: Power Electronics Conference (IPEC), 2010 International, 2010, pp. 746–753. doi:10.1109/IPEC.2010.5544609.

[10] S. Debnath, M. Saeedifard, A new hybrid modular multilevel converter for grid connection of large wind turbines, IEEE Transactions on Sustainable Energy 4 (4) (2013) 1051–1064. doi:10.1109/TSTE.2013.2266280.

[11] S. P. Engel, R. W. D. Doncker, Control of the modular multi-level converter for minimized cell capacitance, in: Power Electronics and Applications (EPE 2011), Proceedings of the 2011-14th European Conference on, 2011, pp. 1–10.

[12] M. Winkelnkemper, A. Korn, P. Steimer, A modular direct converter for transformerless rail interties, in: 2010 IEEE International Symposium on Industrial Electronics, 2010, pp. 562–567.

[13] R. Picas, J. Pou, S. Ceballos, V. G. Agelidis, M. Saeedifard, Minimization of the capacitor voltage fluctuations of a modular multilevel converter by circulating current control, in: IECON 2012 - 38th Annual Conference on IEEE Industrial Electronics Society, 2012, pp. 4985–4991. doi:10.1109/IECON.2012.6388984.

[14] R. Picas, J. Pou, S. Ceballos, J. Zaragoza, G. Konstantinou, V. G. Agelidis, Optimal injection of harmonics in circulating currents of modular multilevel converters for capacitor voltage ripple minimization, in: ECCE Asia Downunder (ECCE Asia), 2013 IEEE, 2013, pp. 318–324. doi:10.1109/ECCE-Asia.2013.6579115.

[15] Q. Tu, Z. Xu, L. Xu, Reduced switching-frequency modulation and circulating current suppression for modular multilevel converters, IEEE Transactions on Power Delivery 26 (3) (2011) 2009–2017. doi:10.1109/TPWRD.2011.2115258.

[16] J. Qin, M. Saeedifard, Predictive control of a modular multilevel converter for a back-to-back hvdc system, IEEE Transactions on Power Delivery 27 (3) (2012) 1538–1547. doi:10.1109/TPWRD.2012.2191577.

[17] L. Harnefors, A. Antonopoulos, S. Norrga, L. Angquist, H.-P. Nee, Dynamic analysis of modular multilevel converters, IEEE Trans. Ind. Electron. 60 (7) (2013) 2526–2537. doi:10.1109/TIE.2012.2194974.

[18] M. Zhang, L. Huang, W. Yao, Z. Lu, Circulating harmonic current elimination of a cps-pwm-based modular multilevel converter with a plug-in repetitive controller, IEEE Transactions on Power Electronics 29 (4) (2014) 2083–2097. doi:10.1109/TPEL.2013.2269140.

[19] D. Jovcic, A. Jamshidi Far, Phasor model of modular multilevel converter with circulating current suppression control, IEEE Trans. Power Del. 30 (4) (2015) 1889–1897. doi:10.1109/TPWRD.2014.2372780.

[20] A. Antonopoulos, L. Angquist, H.-P. Nee, On dynamics and voltage control of the modular multilevel converter, in: 13th European Conf. on Power Electronics and Applicat., 2009. EPE '09., 2009, pp. 1–10.

[21] M. Hagiwara, H. Akagi, Control and experiment of pulsewidth-modulated modular multilevel converters, IEEE Transactions on Power Electronics 24 (7) (2009) 1737–1746. doi:10.1109/TPEL.2009.2014236.

[22] A. Junyent-Ferre, P. Clemow, M. Merlin, T. Green, Operation of hvdc modular multilevel converters under dc pole imbalances, in: 16th European Conf. on Power Electronics and Applicat. (EPE'14-ECCE Europe), 2014, 2014, pp. 1–10. doi:10.1109/EPE.2014.6911011.

[23] L. Angquist, A. Antonopoulos, D. Siemaszko, K. Ilves, M. Vasiladiotis, H. P. Nee, Open-loop control of modular multilevel converters using estimation of stored energy, IEEE Transactions on Industry Applications 47 (6) (2011) 2516–2524. doi:10.1109/TIA.2011.2168593.

[24] M. Guan, Z. Xu, Modeling and control of a modular multilevel converter-based HVDC system under unbalanced grid conditions, IEEE Trans. Power Electron. 27 (12) (2012) 4858–4867.

[25] Q. Tu, Z. Xu, Y. Chang, L. Guan, Suppressing dc voltage ripples of mmc-hvdc under unbalanced grid conditions, IEEE Trans. on Power Del. 27 (3) (2012) 1332–1338. doi:10.1109/TPWRD.2012.2196804.

[26] J.-W. Moon, C.-S. Kim, J.-W. Park, D.-W. Kang, J.-M. Kim, Circulating current control in mmc under the unbalanced voltage, IEEE Trans. on Power Del. 28 (3) (2013) 1952–1959. doi:10.1109/TPWRD.2013.2264496.

[27] M. Vasiladiotis, N. Cherix, D. Siemaszko, A. Rufer, Operation of modular multilevel converters under grid asymmetries, in: 39th Annu. Conf. of the IEEE Ind. Electron. Soc. (IECON), 2013, pp. 6281–6286.

[28] S. Li, X. Wang, Z. Yao, T. Li, Z. Peng, Circulating current suppressing strategy for mmc-hvdc based on nonideal proportional resonant controllers under unbalanced grid conditions, IEEE Trans. on Power Electron. 30 (1) (2015) 387–397. doi:10.1109/TPEL.2014.2329059.

[29] X. Shi, Z. Wang, B. Liu, Y. Liu, L. M. Tolbert, F. Wang, Characteristic investigation and control of a modular multilevel converter-based HVDC system under single-line-to-ground fault conditions, IEEE Trans. on Power Electron. 30 (1) (2015) 408–421.

[30] N. Ahmed, L. Angquist, H.-P. Nee, Continuous modeling of open-loop control based negative sequence current control of modular multilevel converters for HVDC transmission, in: 15th Eur. Conf. on Power Electron. and Appl. (EPE), Lille, France, 2013, pp. 1–10.

[31] X. Li, Q. Song, W. Liu, Q. Li, H. Rao, S. Xu, Zero-sequence voltage injection control scheme of modular multilevel converter supplying passive networks under unbalanced load conditions, Electric Power Syst. Res. 121 (2015) 270 – 278.

[32] S. Cui, S. Kim, J.-J. Jung, S.-K. Sul, A comprehensive cell capacitor energy control strategy of a modular multilevel converter (MMC) without a stiff dc bus voltage source, in: 29th Annu. IEEE Appl. Power Electron. Conf. and Expo. (APEC), Fort Worth, TX, USA, 2014, pp. 602–609.

[33] S. Cui, H.-J. Lee, J.-J. Jung, Y. Lee, S.-K. Sul, A comprehensive ac side single line to ground fault ride through strategy of a modular multilevel converter for HVDC system, in: Energy Conversion Congr. and Expo. (ECCE), Montreal, QC, Canada, 2015, pp. 5378–5385.

[34] J. J. Jung, S. Cui, S. Kim, S. K. Sul, A cell capacitor energy balancing control of modular multilevel converter considering the unbalanced ac grid conditions, in: 2014 International Power Electronics Conference (IPEC-Hiroshima 2014 - ECCE ASIA), 2014, pp. 1268–1275. doi:10.1109/IPEC.2014.6869749.

[35] E. Prieto-Araujo, A. Junyent-Ferre, G. Clariana-Colet, O. Gomis-Bellmunt, Control of modular multilevel converters under singular unbalanced voltage conditions with equal positive and negative sequence components, IEEE Transactions on Power Systems PP (99) (2016) 1–1. doi:10.1109/TPWRS.2016.2598617.

[36] J.-J. Jung, S. Cui, Y. Lee, S.-K. Sul, A cell capacitor energy balancing control of MMC-HVDC under the AC grid faults, in: 9th Int. Conf. on Power Electron. and ECCE Asia (ICPE-ECCE Asia), Seoul, South Korea, 2015, pp. 1–8.

[37] S. Norrga, L. Angquist, K. Ilves, L. Harnefors, H.-P. Nee, Decoupled steady-state model of the modular multilevel converter with half-bridge cells, in: 6th IET Int. Conf. on Power Electron. Machines and Drives (PEMD), Bristol, UK, 2012, pp. 1–6.

[38] G. Buja, G. Indri, Improvement of pulse width modulation techniques, Electrical Engineering (Archiv fur Elektrotechnik) 57 (5) (1975) 281–289.

[39] C. L. Fortescue, Method of symmetrical co-ordinates applied to the solution of polyphase networks, Trans. of the Amer. Institute of Elect. Engineers (2) (1918) 1027–1140. doi:10.1109/T-AIEE.1918.4765570.

[40] H. Akagi, Y. Kanazawa, A. Nabae, Instantaneous reactive power compensators comprising switching devices without energy storage components, IEEE Trans. Ind. Appl. IA-20 (3) (1984) 625–630. doi:10.1109/TIA.1984.4504460.

[41] A. Junyent-Ferre, O. Gomis-Bellmunt, T. Green, D. Soto-Sanchez, Current control reference calculation issues for the operation of renewable source grid interface vscs under unbalanced voltage sags, IEEE Trans. Power Electron. 26 (12) (2011) 3744–3753. doi:10.1109/TPEL.2011.2167761.

[42] H. Akagi, E. Watanabe, M. Aredes, Instantaneous Power Theory and Applications to Power Conditioning, IEEE Press Series on Power Engineering, Wiley, 2007.

[43] L. Shen, M. Barnes, R. Preece, J. Milanovic, K. Bell, M. Belivanis, The effect of vsc hvdc control and operating condition on dynamic behavior of integrated ac/dc system, IEEE Trans Power Del. PP (99) (2015) 1–1. doi:10.1109/TPWRD.2015.2414824.

[44] A. Egea-Alvarez, S. Fekriasl, F. Hassan, O. Gomis-Bellmunt, Advanced vector control for voltage source converters connected to weak grids, IEEE Trans. Power Syst. PP (99) (2015) 1–10. doi:10.1109/TPWRS.2014.2384596.

[45] S. Skogestad, I. Postlethwaite, Multivariable feedback control: analysis and design, Wiley, 1996.

[46] L. Harnefors, H.-P. Nee, Model-based current control of ac machines using the internal model control method, IEEE Trans. Ind. App. 34 (1) (1998) 133–141.

[47] H. Saad, X. Guillaud, J. Mahseredjian, S. Dennetiere, S. Nguefeu, Mmc capacitor voltage decoupling and balancing controls, IEEE Trans. Power Del. 30 (2) (2015) 704–712. doi:10.1109/TPWRD.2014.2338861.

[48] J. Xu, C. Zhao, W. Liu, C. Guo, Accelerated model of modular multilevel converters in pscad/emtdc, IEEE Trans. Power Del. 28 (1) (2013) 129–136. doi:10.1109/TPWRD.2012.2201511.

[49] A. Beddard, M. Barnes, R. Preece, Comparison of detailed modeling techniques for mmc employed on vsc-hvdc schemes, IEEE Trans. Power Del. 30 (2) (2015) 579–589. doi:10.1109/TPWRD.2014.2325065.

[50] Q. Tu, Z. Xu, Impact of sampling frequency on harmonic distortion for modular multilevel converter, IEEE Trans. Power Del. 26 (1) (2011) 298–306. doi:10.1109/TPWRD.2010.2078837.

[51] M. Bollen, L. Zhang, Different methods for classification of three-phase unbalanced voltage dips due to faults, Electric Power Systems Research 66 (1) (2003) 59 – 69, power Quality. doi:http://dx.doi.org/10.1016/S0378-7796(03)00072-5.
URL `http://www.sciencedirect.com/science/article/pii/S0378779603000725`

[52] ENTSO-E, *ENTSO-E network code for requirements for grid connection applicable to all generators*, [Online]. Available: https://www.entsoe.eu [Accessed: Jan. 13, 2016].

[53] The Grid Code, National Grid Electricity Transmission PLC, UK, 2015.

[54] R. Teodorescu, M. Liserre, P. Rodriguez, Grid Converters for Photovoltaic and Wind Power Systems, Wiley - IEEE, Wiley, 2011.